

# Photoionisation cross sections of ultracold $^{88}\text{Sr}$ in $^1\text{P}_1$ and $^3\text{S}_1$ states at 390 nm and the resulting blue-detuned magic wavelength optical lattice clock constraints

MARCIN WITKOWSKI<sup>1,\*</sup>, SŁAWOMIR BILICKI<sup>1</sup>, MARCIN BOBER<sup>1</sup>,  
DOMAGOJ KOVAČIĆ<sup>1,2</sup>, VIJAY SINGH<sup>1</sup>, ARA TONOYAN<sup>1,3</sup>, AND  
MICHAŁ ZAWADA<sup>1</sup>

<sup>1</sup>*Institute of Physics, Faculty of Physics, Astronomy and Informatics, Nicolaus Copernicus University, Grudziądzka 5, PL-87-100 Toruń, Poland*

<sup>2</sup>*Institute of Physics, Bijenička cesta 46, 10000 Zagreb, Croatia*

<sup>3</sup>*Institute for Physical Research, National Academy of Sciences of the Republic of Armenia, Ashtarak-2, 0203, Armenia*

\**marcin\_w@umk.pl*

**Abstract:** We present the measurements of the photoionisation cross sections of the excited  $^1\text{P}_1$  and  $^3\text{S}_1$  states of ultracold  $^{88}\text{Sr}$  atoms at 389.889 nm wavelength, which is the magic wavelength of the  $^1\text{S}_0$ - $^3\text{P}_0$  clock transition. The photoionisation cross section of the  $^1\text{P}_1$  state is determined from the measured ionisation rates of  $^{88}\text{Sr}$  in the magneto-optical trap in the  $^1\text{P}_1$  state to be  $2.20(50)\times 10^{-20}$  m<sup>2</sup>, while the photoionisation cross section of  $^{88}\text{Sr}$  in the  $^3\text{S}_1$  state is inferred from the photoionisation-induced reduction in the number of atoms transferred through the  $^3\text{S}_1$  state in an operating optical lattice clock to be  $1.38(66)\times 10^{-18}$  m<sup>2</sup>. Furthermore, the resulting limitations of employing a blue-detuned magic wavelength optical lattice in strontium optical lattice clocks are evaluated. We estimated photoionisation induced loss rates of atoms at 389.889 nm wavelength under typical experimental conditions and made several suggestions on how to mitigate these losses. In particular, the large photoionisation induced losses for the  $^3\text{S}_1$  state would make the use of the  $^3\text{S}_1$  state in the optical cycle in a blue-detuned optical lattice unfeasible and would instead require the less commonly used  $^3\text{D}_{1,2}$  states during the detection part of the optical clock cycle.

© 2022 Optica Publishing Group under the terms of the Optica Open Access Publishing Agreement

## 1. Introduction

Optical atomic clocks have proven to be excellent research instruments in various fields ranging from ultra-precise metrology [1–5], tests of fundamental physics [5, 6] to searches for new matter in astrophysics [7–10]. Along with improving atomic optical clocks, the factors limiting their performance have become increasingly important. The perturbing effects induced by the environment, like light shifts [11], black-body radiation (BBR) shifts [12], and collisional shifts [13], are matters of growing experimental concern. Several solutions have been implemented to counteract these undesirable effects, like Pauli blocking mechanism [14, 15], temperature decreasing through cryogenic systems [16], and light shift cancellation by magic-wavelength-based optical traps [17, 18].

A blue-detuned optical trap has been proposed as an alternative to commonly used red-detuned optical traps [19]. In blue-detuned optical traps, atoms are confined near the minimum of light intensity, leading to a significant reduction of light-induced perturbations. On the other hand, if the energy of the blue-detuned trapping light photon is above the atomic ionisation threshold, it may lead to atomic losses. Moreover, they were proposed together with the red-detuned conveyor belt optical lattice as a way to realise an active optical atomic clock based on superradiance [20].

In the present work, we analyse the feasibility of the blue-detuned magic wavelength for the optical trapping of strontium atoms and possible atomic losses due to photoionisation.

A blue-detuned magic wavelength for the  $^1S_0$ - $^3P_0$  clock transition in  $^{87}\text{Sr}$  was experimentally determined to be 389.889(9) nm [19]. While these blue-detuned magic wavelength photons do not have sufficient energy to ionise the atoms directly from the strontium clock ( $^1S_0$  and  $^3P_0$ ) states, other states that are involved during the normal operation of the strontium optical lattice clock are potentially affected by the photoionisation (see the region between the dashed lines in Fig. 1). For instance, the first stage of cooling down the atoms before loading them into the optical lattice is generally based on the  $^1S_0$ - $^1P_1$  transition (460.9 nm in Fig. 1), and the repumping during detection is based on the  $^3P_0$ - $^3S_1$  and  $^3P_2$ - $^3S_1$  transitions (679.3 nm and 707.2 nm, respectively, in Fig. 1) [21–23].

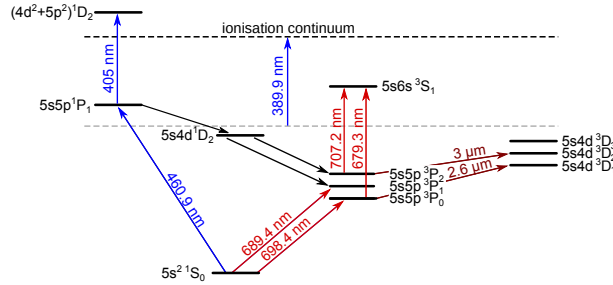


Fig. 1. Schematic energy level diagram showing relevant optical transitions used in the basic cycle of a strontium optical lattice clock. The 460.9 nm transition is used in the first stage of cooling and for imaging of atoms. The 689.4 nm transition is used in the next cooling stages and the optical pumping in fermionic isotopes. The 707.2 nm and 679.3 nm transitions are used to repump the  $^3P_0$  and  $^3P_2$  states. The 698.4 nm transition is the clock transition. The 405 nm wavelength corresponds to the autoionisation resonance  $(4d^2+5p^2)^1D_2$ . The states belonging to the area bounded by the dashed lines are potentially affected by the photoionisation light at 389.9 nm. The 3  $\mu\text{m}$  and 2.6  $\mu\text{m}$  transitions can be used as an alternative repumping scheme.

To determine photoionisation cross sections for  $^1P_1$  and  $^3S_1$  levels, we used two different experimental methods. To investigate the photoionisation effect on the  $^1P_1$  state, we compared the dynamics of loading atoms into the magneto-optical trap (MOT) with and without the ionising blue-detuned magic wavelength 389.889 nm light, alternately. To measure the photoionisation cross section for  $^3S_1$  state, we detect atomic losses from the optical lattice trap induced by the presence of an ionisation laser beam at blue-detuned magic wavelength during the strontium optical lattice clock operation. The results of both measurements were used to analyse how the photoionisation by the blue-detuned magic wavelength light affects the performance of the optical atomic clocks under typical experimental conditions. Since the magic wavelength does not depend heavily on the particular isotope, as was shown for the red-detuned magic wavelength of Sr at 813 nm [24], we based our research on a more abundant bosonic  $^{88}\text{Sr}$  isotope without limiting the generality of our results.

## 2. Experiment

### 2.1. Experimental setup

The photoionisation experiment has been performed on the Sr optical lattice atomic clock setup described in detail in [25] operating on  $^{88}\text{Sr}$  bosonic isotope. A basic cycle of this clock consists of cooling and loading atoms into a 1D red-detuned optical lattice trap, an interrogation of the clock transition by an ultra-stable clock laser, and detection of the resulting atomic population

in the ground ( $^1S_0$ ) and the excited ( $^3P_0$ ) clock states [21]. Cooling and loading of atoms into the optical lattice trap are achieved by two consecutive MOTs, operating on the  $^1S_0$ - $^1P_1$  (blue MOT) and  $^1S_0$ - $^3P_1$  (red MOT) transitions, respectively. The clock  $^1S_0$ - $^3P_0$  transition is interrogated by the  $\pi$ -pulse Rabi excitation. The clock cycle is concluded by the detection phase that measures the ratio of populations in  $^1S_0$  and  $^3P_0$  states with the help of an electron shelving scheme [26], including fluorescence imaging on  $^1S_0$ - $^1P_1$  transition and optical pumping on  $^3P_0$ - $^3S_1$  and  $^3P_2$ - $^3S_1$  transitions.

The photoionisation laser beam is synthesised via frequency doubling of a TiSa tunable laser light inside a bow-tie enhancement cavity. The resulting laser beam is spatially filtered with polarisation-maintaining single-mode fibre and expanded by sets of lenses to either  $\sigma_x=7.034(85)$  mm and  $\sigma_y=6.07(30)$  mm or  $\sigma_x=2.19(11)$  mm and  $\sigma_y=1.88(12)$  mm beam waist radii and directed on atoms trapped by the blue MOT or the optical lattice trap, respectively. The diameter of the ionisation beam is much larger than the typical dimensions of atomic clouds, i.e.,  $2.4 \text{ mm} \times 2.4 \text{ mm}$  and  $157 \mu\text{m} \times 66 \mu\text{m}$  for blue MOT and the optical lattice, respectively. The frequency of the ionising laser is stabilised to a wavemeter through an analogue feedback loop with an accuracy better than 100 MHz.

## 2.2. Photoionisation of the $^1P_1$

To determine photo-induced losses from the  $^1P_1$  state due to blue-detuned magic 389.889 nm light, we analysed the fluorescence signal at 461 nm emitted by  $^{88}\text{Sr}$  atoms during the blue MOT loading phase. To ensure that the  $^1P_1$  is the only possible ionised state, the repumping laser beams for the  $^3P_0$  and  $^3P_2$  states were switched off (see Fig. 1). The photoionisation cross section  $\sigma_{1P_1}$  was determined by comparing the loading rates of the MOT fluorescence with and without the photoionising 389.889 nm light. This technique has proven very efficient in measuring absolute ionisation cross sections of trapped atoms [27, 28].

The rate equation for the number of atoms  $N_{\text{Sr}}$  loaded into the MOT can be expressed as [29]

$$\frac{dN_{\text{Sr}}}{dt} = L_{\text{Sr}} - (\gamma_{\text{Sr}} + \gamma_P) N_{\text{Sr}} - \beta_{\text{SrSr}} \int dr^3 n_{\text{Sr}}^2, \quad (1)$$

where  $L_{\text{Sr}}$  is the MOT loading rate,  $\gamma_{\text{Sr}}$  is the combined loss coefficient due to collisions with background gases, optical pumping to the metastable states and other possible single atom losses,  $\gamma_P$  is the loss coefficient due to photoionisation,  $\beta_{\text{SrSr}}$  is the loss coefficient due to light-assisted collisions between Sr atoms, and  $n_{\text{Sr}}$  is the spatial density of trapped atoms. In this approach, photoionisation is considered as another mechanism of losses, linearly dependent on the number of atoms. The approach is valid if the photoionising beam does not modify the density distribution of the MOT (e.g. by a dipole force), which is always fulfilled in our setup.

The experiment was performed in the low-density regime, which means that the mean free path of the atoms is larger than the size of the trapped atomic cloud. A typical number of strontium atoms in a blue MOT of a diameter of  $\sim 2$  mm is  $\sim 6 \times 10^8$  [25]. It gives an atomic density of  $\sim 10^{11} \text{ cm}^{-3}$ . Using the  $^{88}\text{Sr}$  collision cross-section of  $10^{-13} \text{ cm}^2$  [30], the mean free path of the atoms trapped in the blue MOT is  $\sim 100$  cm, which is very large compared to the size of the MOT. The low-density regime enables us to neglect the last term in Eq. (1) as the collisions between trapped atoms are negligible. This yields the simplified rate equation

$$\frac{dN_{\text{Sr}}}{dt} = L_{\text{Sr}} - (\gamma_{\text{Sr}} + \gamma_P) N_{\text{Sr}}. \quad (2)$$

Integration of Eq. (2) over time gives the formula for the dependence of the number of atoms on time during MOT loading

$$N_{\text{Sr}}(t) = \frac{L_{\text{Sr}}}{\gamma_{\text{Sr}} + \gamma_P} (1 - \exp(-(\gamma_{\text{Sr}} + \gamma_P)t)), \quad (3)$$

where  $N_{Sr}(t = 0) = 0$ .

The loss coefficient  $\gamma_P$  is related to the intensity  $I_P$  of the ionising light through the expression

$$\gamma_P = \rho_{1P_1} \sigma_{1P_1} \frac{I_P}{h\nu_P}, \quad (4)$$

where  $\rho_{1P_1}$  is the fraction of atoms in  $^1P_1$  excited state,  $\sigma_{1P_1}$  is the photoionisation cross section, and  $I_P/h\nu_P$  is the ionising photon flux. The frequency  $\nu_P$  is determined with the type B standard uncertainty  $u(\nu_P)$  derived from the accuracy of the wavemeter. To find the value of the  $\gamma_P$  coefficient, two blue MOT loading curves were recorded sequentially in the presence and absence of the photoionisation laser beam (see Fig. 2). By fitting Eq. (3) independently to both curves, we obtained loading rates  $\gamma_{Sr}$  and  $\gamma_{Sr} + \gamma_P$ , and determined  $\gamma_P$  by their difference. The typical loading curves detected in the experiment are presented in Fig. 3. For these curves, the loss coefficients are  $\gamma_{Sr} = 34.08(80) \text{ s}^{-1}$  and  $\gamma_{Sr} + \gamma_P = 37.9(1.5) \text{ s}^{-1}$ , which corresponds to the reduction of the  $1/e$  MOT loading time from 29.34(69) ms to 26.4(1.0) ms. To block the scattered light from the ionisation laser, the blue MOT fluorescence was filtered by a 461 nm interference filter and then focused on a photodiode.

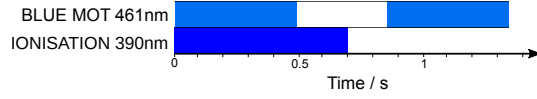


Fig. 2. The timing sequence of the lasers used in the  $^1P_1$  photoionisation experiment. The time of the blue MOT's loading phase is identical in each sequence. To record the background from the ionisation laser beam, it was kept on for a 200 ms longer compared to MOT's loading phase duration.

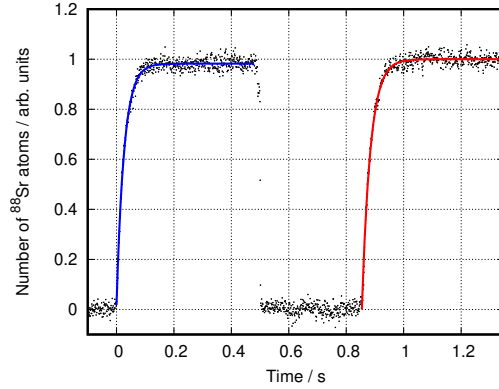


Fig. 3. Typical fluorescence of  $^{88}\text{Sr}$  atoms detected while loading into the blue MOT in the presence (left) and in the absence (right) of the photoionising 389.889 nm light. The solid blue and red lines depict fitted Eq. (3).

To determine the fraction of atoms in the excited state  $\rho_{1P_1}$ , a model for two-level system was used

$$\rho_{1P_1} = \frac{1}{2} \frac{I_{461}/I_{sat}}{I_{461}/I_{sat} + 4(\Delta/\Gamma)^2 + 1}, \quad (5)$$

where  $I_{461}$  is the total intensity of the blue MOT trapping laser light,  $I_{sat}$  is the  $^1S_0$ - $^1P_1$  transition saturation intensity ( $427 \text{ W/m}^2$ ),  $\Gamma$  is the natural decay rate of the excited  $^1P_1$  state ( $2\pi \times 32 \text{ MHz}$ )

and  $\Delta$  is the trapping laser detuning from resonance (typically  $2\Gamma$ ). The population fraction of the atoms in  $^1P_1$  state was varied by changing the trapping laser intensity. To calibrate the trapping laser intensity, a small portion of the trapping 461 nm laser light was uncoupled before splitting and sent to a photodetector to monitor the intensity  $I_{461}$ .

The detuning  $\Delta$  was continuously measured by an optical frequency comb. The related uncertainties  $u(I_{461})$  and  $u(\Delta)$  were determined as standard deviations of their means. The intensity of the trapping laser light and its detuning from the resonance were continuously recorded by data acquisition software. The trapping beam is expanded to a diameter of 2 cm and is split into three retro-reflected beams. The typical value of the total intensity of the blue MOT trapping laser light seen by atoms, taking into account losses on viewports and optics, is  $I_{461} = 6 \times 30 \text{ W/m}^2 \approx 0.42 I_{sat}$ . The methods that calibrate population dependence on the MOT beams intensity, described e.g. in [28, 31], are not used here since they require laser light intensities exceeding the saturation of the transition. Instead, the measured values of  $I_{461}$  and  $\Delta$  are directly used in Eq. (5).

### 2.3. Photoionisation of the $^3S_1$

To measure the photoionisation cross section of  $^3S_1$  state at 389.889 nm, we employed a different experimental approach. The experiment was performed during the standard clock cycle of the strontium optical lattice clock described in detail elsewhere [25]. The timing sequence of the laser beams used in the experiment is shown in Fig. 4. After sequential cooling in blue and red MOT Sr, atoms are transferred into the 1D vertical red-detuned magic wavelength optical lattice at 813 nm and interrogated by an ultrastable clock laser. The clock laser is locked to the  $^1S_0$ - $^3P_0$  transition in the second, independent strontium optical lattice clock. The clock laser interrogation pulse, long with respect to the transition Rabi frequency, is applied exactly on the transition centre frequency and excites one-half of the atoms ( $N_e$ ) to the  $^3P_0$  state while the rest of the atoms ( $N_g$ ) remain in the ground  $^1S_0$  state. Subsequently, after that, Sr atoms initially excited to the  $^3P_0$  state are pumped back to the ground state through the  $^3S_1$ ,  $^3P_1$ , and  $^3P_2$  states with 679.3 nm and 707.2 nm transitions (see Figs. 1 and 4). The number of previously excited atoms  $N_e$  is then determined by the second imaging pulse at 461 nm. The detection is concluded by a background image of the empty trap.

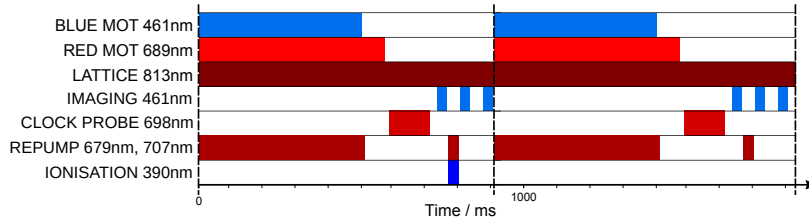


Fig. 4. The timing sequence of the lasers used in the  $^3S_1$  photoionisation experiment. It consists of two clock cycles, the first one (left) with an added photoionising pulse, the second one (right) providing a background.

A pulse of the photoionising beam added during the repumping phase of the first clock cycle opens a new channel of losses due to photoionisation from the  $^3S_1$  state. Therefore, it decreases repumping efficiency and, consequently, reduces the number of atoms recorded by the second imaging pulse. The photoionisation cross section  $\sigma_{^3S_1}$  is inferred from the photoionisation-induced reduction in the number of atoms  $\Delta N_e = N_e - N_e^I$ , where  $N_e^I$  and  $N_e$  are the excited-state  $^3P_0$  populations detected sequentially in the presence (the first cycle in Fig. 4) and absence of the photoionisation beam (the second cycle in Fig. 4), respectively.

### 3. Results

#### 3.1. Photoionisation cross section at blue magic wavelength

The photoionisation cross section  $\sigma_{1P_1}$  was determined from the loss coefficient  $\gamma_P$  and characteristics of both the blue MOT and the ionising beam. The atomic distribution in the blue MOT detected by a CCD camera is well described by the Gaussian-like profile

$$N(x, y) = \frac{2N_0}{\pi r_x r_y} \exp\left(\frac{-2x^2}{r_x^2}\right) \exp\left(\frac{-2y^2}{r_y^2}\right), \quad (6)$$

where  $r_x, r_y$  are MOT radii (about 1.2 mm, typically). The averaged intensity of the ionising light  $\langle I_P \rangle$  seen by atoms in the blue MOT is given by

$$\langle I_P \rangle = \int \int \frac{I(x, y)N(x, y)}{N_0} dx dy, \quad (7)$$

where  $N_0$  is the total number of atoms in the MOT, and  $I(x, y)$  and  $N(x, y)$  are distributions of the intensity of the beam and the atoms, respectively. The intensity profile of the photoionising beam was determined by a CCD beam profiler measurement and corrected with the coefficient of transmission through the vacuum chamber viewports. The intensity of the ionising light was power-locked and continuously monitored by a photodiode, and the related uncertainty  $u(I_P)$  was calculated as a standard error of the mean of the recorded photodiode readout. The photodiode was calibrated based on the uncertainties related to the atomic distribution, namely  $u(r_x)$  and  $u(r_y)$ .

The photoionisation cross section  $\sigma_{1P_1}$  was calculated according to Eq. (4) by combining the measured values of the excited state fraction  $\rho_{1P_1}$ , loss coefficient  $\gamma_P$ , and the intensity  $\langle I_P \rangle$ , monitored and recorded during measurements. We recorded 12 to 20 pairs of MOT loading curves sequentially with (the first curve) and without the photoionisation beam (the second curve) for each wavelength of the photoionisation beam separately. For each pair of curves, we determined the ionisation loss rate  $\gamma_P$  as the difference  $(\gamma_{Sr} + \gamma_P) - \gamma_{Sr}$ , where  $\gamma_{Sr} + \gamma_P$  and  $\gamma_{Sr}$  were determined by fitting the Eq. (3) to the first or the second curve, respectively. The uncertainty  $u(\gamma_P)$  was calculated independently for each wavelength as the standard deviation of the mean. Finally, the uncertainty of the photoionisation cross section  $u(\sigma_{1P_1})$  was calculated as a combined standard uncertainty with several independent quantities, namely  $u(\gamma_P)$ ,  $u(I_P)$ ,  $u(\Delta)$ ,  $u(I_{461})$ , and  $u(\nu_p)$ .

To verify our experimental method, we extended the range of photoionisation wavelengths to cover the autoionisation resonance  $(4d^2 + 5p^2)^1D_2$  near 405 nm [32–34]. This way, we enabled comparison with previous measurements of the autoionisation resonance performed with different experimental approaches [35, 36]. The measurements of  $\sigma_{1P_1}$  were carried out for wavelengths in a range from 378.4 nm to 407 nm. The results are shown in Fig. 5.

By fitting a Fano profile [37] to the measured points, we determined the position of the resonance and its peak value to be  $\lambda_R = 405.196(44)$  nm and  $\sigma_R = 5.20(94) \times 10^{-19}$  m<sup>2</sup>, respectively. To exclude another possible resonance observed on the high energy wing of the measured photoionisation spectra, the fitting range was limited to the experimental points above 392 nm. The gap in results between 390 nm and 392 nm is due to technical problems related to the locking of TiSa laser within the corresponding range. Our results are consistent with the results presented previously by Mende et al. ( $\lambda_R = 405.213(2)$  nm,  $\sigma_R = 5.6(1.1) \times 10^{-19}$  m<sup>2</sup>) [35] and by Sami-ul-Haq et al. ( $\lambda_R = 405.177(16)$  nm,  $\sigma_R = 5.45(98) \times 10^{-19}$  m<sup>2</sup>) [36]. Note that previous measurements, unlike ours, did not involve cold atomic samples.

At the blue magic 389.889 nm wavelength, the photoionisation cross section is equal to  $2.20(50) \times 10^{-20}$  m<sup>2</sup> (see Fig. 5). Our result is consistent with the value deduced from the curve reported by Mende et al. [35]  $1.46(29) \times 10^{-20}$  m<sup>2</sup>, within the 20% uncertainty claimed by the

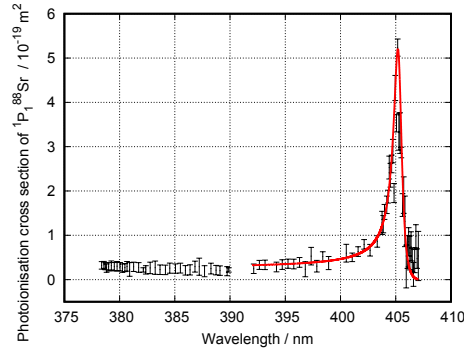


Fig. 5. The photoionisation cross section from the  $^1P_1$  state as a function of the wavelength of the ionising light. The solid red line is a Fano profile fitted to the measured data. The fitting range is limited to the experimental points above 392 nm to exclude another possible resonance below 389.9 nm.

author. In our case, the most significant factor contributing to the uncertainty of  $\sigma_{^1P_1}$  comes from the fluctuation of the number of atoms loaded into the blue MOT. The atom number fluctuation affects the fitting uncertainty, however, as the statistical error, it is averaged, and it does not contribute to the final result, only to its uncertainty.

In the second set of experiments, the photoionisation cross section from the  $5s6s^3S_1$  excited state was determined by

$$\sigma_{^3S_1} = \frac{\langle \Delta N_e \rangle}{\langle N_e \rangle} \frac{h\nu_P}{\langle I_P \rangle t_{\text{int}}}, \quad (8)$$

where  $\langle N_e \rangle$  and  $\langle \Delta N_e \rangle$  are the averaged excited state  $^3P_0$  population and its averaged photoionisation-induced reduction during the repumping through the  $^3S_1$  state, respectively,  $\langle I_P \rangle$  is the averaged intensity of the photoionisation radiation seen by atoms in the optical lattice calculated according to Eq. (7), and  $t_{\text{int}}$  is the interaction time between photoionisation beam and the atoms in the  $^3S_1$  state. The value of  $t_{\text{int}} = 43$  ns was determined on the basis of both  $^3S_1 \rightarrow ^3P_2$  and  $^3S_1 \rightarrow ^3P_0$  transition probabilities [38] and the natural lifetime of the  $^3S_1$  state [39, 40]. Additionally, in calculating the interaction time  $t_{\text{int}}$ , we included repumping to the excited  $^3S_1$  state back from  $^3P_2$  and  $^3P_0$  states. The ionisation beam was power-locked with an intensity of  $26270(80)$  W/m<sup>2</sup> at the Gaussian-profile peak. The  $e^{-2}$  diameters of the beam ( $2.19(11) \times 1.88(12)$  mm) are much larger than the dimensions of the illuminated atomic cloud ( $157(10)$   $\mu\text{m} \times 66(6)$   $\mu\text{m}$ ). To ensure the stability of the number of atoms throughout each experimental cycle, we monitored both ground-state populations  $N_g$  and  $N_g^I$  independently. The experimental points satisfying the relation  $(N_g - N_g^I)/N_g > 2\%$  were excluded resulting in 3292 points left for further analysis. To be less prone to the oscillations of the number of atoms, we made the interleaved measurements randomly staggered by the manual triggering of consecutive cycles.

The determination of the cross section  $\sigma_{^3S_1}$  based on Eq. (8) yields  $\sigma_{^3S_1} = 1.38(66) \times 10^{-18}$  m<sup>2</sup>. The uncertainty of the  $\sigma_{^3S_1}$  was calculated as the combined standard uncertainty involving the uncertainties  $u(\langle N_e \rangle)$ ,  $u(\langle \Delta N_e \rangle)$ ,  $u(\langle I_P \rangle)$ , and  $u(\nu_P)$ . The frequency type B uncertainty  $u(\nu_P)$  is derived from the resolution of the wavemeter. All the other terms are calculated as the standard deviations of their means.

### 3.2. Study of feasibility: strontium optical clock with blue-detuned magic wavelength optical lattice

In this section, we use our measured photoionisation cross sections of  $^1P_1$  and  $^3S_1$  states to estimate the impact of the loss of the atoms from these states due to the ionisation in a blue-detuned magic wavelength optical lattice on an optical strontium clock operation and suggest possible mitigation measures.

As mentioned above, in a blue-detuned magic wavelength optical lattice, atoms are confined at the minima of light intensity as opposed to a red-detuned magic wavelength optical lattice. However, the atoms cannot be trapped in a simple 1D blue-detuned magic wavelength lattice trap because they will escape along the radial directions. Confinement in all three orthogonal directions can be achieved, for instance, by a 3D optical lattice trap, made up of three independent 1D optical lattices [41]. Moreover, a 3D optical lattice will reduce the influence of interactions between atoms on the optical clock's accuracy [42].

To reach the accuracy goal of state-of-the-art optical lattice clocks, all frequency shifts connected with motional effects must be suppressed. When each atom is confined in a single lattice site to a region much smaller than the wavelength of the clock probing laser, and any tunnelling between sites is negligible, the Doppler and recoil shifts are suppressed, and the atoms are in the Lamb-Dicke regime [43,44]. This implies different limits on minimal required potential depth depending on the direction of the probing of the clock transition by a clock laser beam, either horizontal or vertical. On the other hand, higher potential means higher losses due to photoionisation.

#### 3.2.1. Horizontal direction

In a horizontal periodic potential, the states with the same vibrational quantum number in different potential wells are degenerated in energy, amplifying tunnelling between the wells. This will spread out the spatial wave functions of the atoms so that they are not localised to a single well and create a band structure in their energy spectrum. This yields, depending on the initial state of the atoms in the trap, a broadening and a shift of the atomic transition of the order of the bandwidth of the lowest energy band of the system [45]. Figure 3 of [45] shows the corresponding bandwidth with the bandwidth in units of the recoil energy  $E^{\text{rec}}$  associated with the absorption or emission of a photon of the lattice light and in Hz units calculated for 813 nm magic wavelength.

Since the recoil energy scales like  $k^2$ , where  $k$  is the wavenumber of the lattice light, in the blue-detuned lattice, for instance, the bandwidth of  $\sim 1$  mHz, corresponding to the  $10^{-17} - 10^{-18}$  accuracy range, requires the potential depth above  $\sim 125 E^{\text{rec}}$ .

#### 3.2.2. Vertical direction

For a vertical clock laser probe beam, the approach from the previous subsection is no longer valid due to the presence of gravity. In the periodic potential in an accelerated frame, energies of atoms in adjacent lattice sites are shifted, and the Hamiltonian no longer supports bound states. This means that an atom in a vertical optical lattice will eventually tunnel to a continuum. Fortunately, the timescale of this process increases exponentially with lattice depth [45], and this is not an issue with the lattice depths considered here. Therefore, we must adopt the formalism of Wannier-Stark states [46]. The external Hamiltonian of an atom with mass  $m$  in a vertical lattice optical trap of the depth  $U_{0z}$  is given as

$$\hat{H} = \frac{\hbar^2 \kappa^2}{2m} + \frac{U_{0z}}{2} [1 - \cos(2k\hat{z})] + mg\hat{z}, \quad (9)$$

where  $\kappa$  is the atom quasimomentum in  $z$ -direction. The eigenstates of this Hamiltonian are called Wannier-Stark states  $|W_M\rangle$ , where  $M$  denotes  $m$ th well of the lattice. We have constructed the Wannier-Stark state as the sum of Wannier states in different lattice sites (i.e. the eigenstates

of Hamiltonian in Eq. (9) without gravity) where every Wannier function is weighed by the appropriate Bessel function [47]. Fig. 6 shows the spatial representation of Wannier-Stark states  $|W_0\rangle$  centred around site  $M = 0$  for different values of the lattice depth  $U_{0z}$ . The states are calculated for 390 nm blue-detuned lattice and, for comparison, for widely-used 813 nm red-detuned lattice. In both cases, we assumed that the tunnelling between different energy bands is negligible, i.e. the atom can only tunnel between lattice sites of the ground energy band.

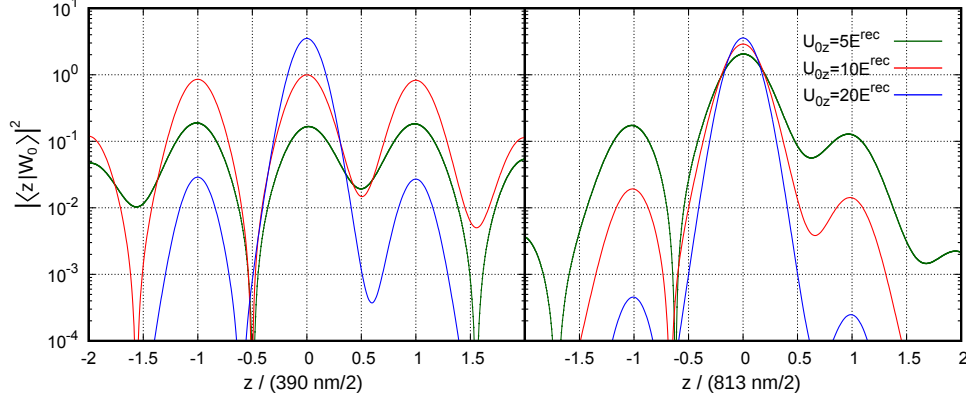


Fig. 6. Wannier-Stark states in position representation for different lattice depths for 390 nm (left) and 813 nm (right) magic wavelength lattices.

As seen in Fig. 6, for an 813 nm red-detuned optical lattice, the Wannier-Stark state consists of a main central peak and two smaller "revival" peaks in the adjacent wells, even for shallow lattices. These revival peaks decay quickly with increasing lattice depth, with revival peaks being hundred times smaller at lattice depths of  $10 E_z^{\text{rec}}$  and the wave function being practically localised to one lattice site [45]. To achieve similar ratios of the main and side peaks for a 390 nm blue-detuned lattice, the lattice should be at least twice as deep, i.e.  $U_{0z} = 20 E^{\text{rec}}$  because of the shorter distance between lattice sites and thus smaller energy shifts in the adjacent sites.

To examine the effects of coupling the Wannier-Stark states to their neighbours by the  $^1S_0$ - $^3P_0$  probe beam, we consider the Wannier-Stark ladder of states with an internal two-level energy structure ( $|g, W_M\rangle, |e, W'_M\rangle$ ). The Wannier-Stark ladder is a set of Wannier-Stark states with one  $|W_M\rangle$  state in each lattice site. Wannier-Stark states in the adjacent lattice sites are separated in energy by  $\hbar\Delta_g$  corresponding to the change in gravitational potential between sites. For Sr, this separation between adjacent sites is equal to  $\frac{\Delta_g}{2\pi} = 417$  Hz for 390 nm blue-detuned lattice. The energy difference between the ground  $|g\rangle$  state and the excited  $|e\rangle$  state of the atom is given by  $\hbar\omega_{eg}$ . The probe beam couples the  $|g, W_M\rangle$  and  $|e, W'_M\rangle$  states with different coupling strengths  $\Omega_{\Delta M}$ , where  $\Delta M = M' - M = 0$  and  $\Delta M \neq 0$  for coupling of WS states in the same lattice site and for coupling to neighbouring lattice sites, respectively. This coupling corresponds to a translation in momentum space  $e^{ik_c z}$  [45]:

$$\Omega_{\Delta M} = \Omega \langle W_M | e^{ik_c \hat{z}} | W_{M'} \rangle, \quad (10)$$

where  $k_c$  is the wavevector of the coupling probe laser and  $\Omega$  is the Rabi frequency. The relative coupling strengths  $|\frac{\Omega_{\Delta M}}{\Omega}|^2$  of the "carrier"  $\Omega_0$  and the first 4 "sidebands"  $\Omega_{\pm 1, \pm 2}$  as a function of lattice depth are shown in Fig. 7 (left). For very shallow optical lattices with depths below  $15 E^{\text{rec}}$  the couplings show strong oscillations similar to those in [48]. For higher lattice depths, couplings to neighbouring lattice sites rapidly decay and the atom becomes trapped in a single lattice with strong suppression of tunnelling between sites. Additionally, Fig. 7 (left) shows that for shallow lattice it is possible to choose different ratios of coupling parameters  $\frac{\Omega_0}{\Omega_{1,2}}$  by tight

control of lattice depth. This control over coupling parameters allows engineering of the extent of atomic wavefunctions through the adjustment of trap depth and thereby lowering the collisional frequency shifts arising from the on-site p-wave and neighbouring-site s-wave interactions, as done for 813 nm optical lattice [49]. For lattice depth of  $20E^{\text{rec}}$ , coupling strengths to the nearest and second-nearest lattice site are  $10^{-2}$  and  $10^{-4}$  times weaker than coupling between the ground  $|g, W_M\rangle$  and excited  $|g, W_M\rangle$  WS state in the same lattice site.

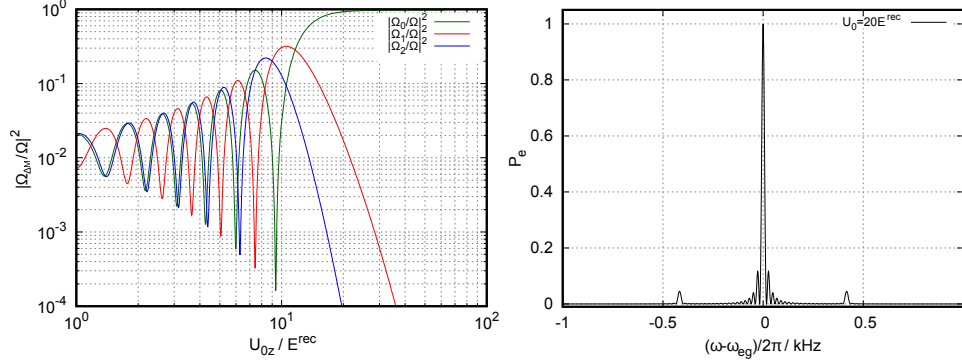


Fig. 7. (left) Relative coupling strengths  $|\frac{\Omega_{\Delta M}}{\Omega}|^2$  of the carrier ( $\Delta M = 0$ ) and first 4 sidebands ( $\Delta M = \pm 1, \Delta M = \pm 2$ ) as a function of lattice depth for a blue-detuned optical lattice. (right) Transition probability  $P_e$  of the  $^1S_0$ - $^3P_0$  clock transition for effective Rabi frequency  $\Omega_0/2\pi = 10$  Hz and  $\pi$ -pulse interaction time of 50 ms when the initial state is a pure Wannier-Stark state and  $U_0 = 20 E^{\text{rec}}$ .

To calculate the populations of the ground and excited WS states, we considered the evolution of the different states under coupling to the probe laser by numerically solving the set of differential equations [45]

$$\begin{aligned} i\dot{a}_M^g &= \sum_{M'} \frac{\Omega_{M-M'}^*}{2} e^{-i\pi M' k_c/k} e^{i\Delta_{M-M'} t} a_{M'}^e, \\ i\dot{a}_M^e &= \sum_{M'} \frac{\Omega_{M'-M}}{2} e^{i\pi M k_c/k} e^{-i\Delta_{M'-M} t} a_{M'}^g, \end{aligned} \quad (11)$$

where  $a_M^g$  and  $a_M^e$  are the probability amplitudes of the ground and excited state, respectively, and  $\Delta_{M-M'} = \omega - \omega_{eg} + (M - M')\Delta_g$ . In these calculations we assume that the atom can only tunnel to the nearest lattice site and the initial state is a pure WS state.

The computed resonances for a blue-detuned vertical optical lattice with depth of  $20E^{\text{rec}}$ , an effective Rabi frequency  $\Omega_0/2\pi = 10$  Hz and interaction time of 50 ms are shown in Fig. 7 (right). The central resonance corresponds to the clock transition frequency  $\omega_{eg}$  and two frequency sidebands located at  $\pm\Delta_g/2\pi$  arise from weak tunnelling of atoms to neighbouring sites and are completely symmetric with respect to the central resonance.

The results presented in Figs. 7 shows that the blue-detuned vertical lattice with depth of  $20E^{\text{rec}}$  has similar level of suppression of the tunnelling and of the effects of the atom dynamics as the  $10E^{\text{rec}}$  deep red-detuned optical lattice [45]. To hold the atoms in a 3D blue-detuned magic lattice, it is required that the energies of the first few lattice states are smaller than the lattice depth. The  $20 E^{\text{rec}}$  trap depth corresponds to around 14  $\mu\text{K}$  and it is sufficiently deep to hold atoms cooled down by using the  $^1S_0$ - $^3P_1$  (red MOT) transition — typical temperatures achieved in the last cooling stage are of the order of 1  $\mu\text{K}$ .

### 3.2.3. Photoionisation losses due to blue magic lattice

The previous subsections show that the minimal required optical trap potential depth for an effective operation of an optical strontium clock based on the blue-detuned 390 nm magic wavelength is on the order of  $20 E^{\text{rec}}$ , assuming vertical probing of the clock transition. Now we want to estimate the losses due to the presence of the 3D blue-detuned lattice potential during a commonly used optical strontium clock operation cycle.

To characterise the photoionisation losses, we consider two parts of the clock cycle when atoms are being cooled and trapped by the blue MOT and when the atoms are already loaded into the optical lattice. We assume that the 3D lattice potential is present during the whole clock cycle.

#### Atoms trapped in the blue MOT

The photoionisation losses can lower the total number of the atoms loaded into the blue MOT, which would decrease the number of atoms transferred into the 3D optical lattice trap and consequently lower the signal-to-noise ratio of the observed clock line. In the blue MOT phase atoms are cooled and trapped through the  $^1P_1$  state. About 0.002% of atoms escape the closed cooling transition  $^1S_0 \leftrightarrow ^1P_1$  and must be repumped. Typically, the repumping through the  $^3S_1$  state is chosen [50]. However, as the photoionisation of the  $^3S_1$  state by the blue-detuned light at 390 nm is significant, a different repumping scheme, e.g., through the  $^3D$  state [51, 52], is preferable.

In most of the present realisations of optical lattice clock, the centres of the blue MOT and the lattice trap overlap and the waist of the 1D optical lattice is much smaller than the atomic cloud trapped in the blue MOT. At the same time, with some notable exceptions [53], the optical lattice is shallow in comparison with the temperature of blue MOT atoms and they can freely pass the optical lattice area. Therefore, any losses due to photoionisation in the blue MOT due to the blue magic 3D lattice can appear only when atoms are passing the optical lattice region.

To estimate the losses, we assume a typical blue MOT condition with maximum total intensity of the trapping beams equal to  $I_{461} = 6 \times 30 \text{ W/m}^2$  and their detuning from atomic resonance  $\Delta = 1.25\Gamma$ , and use Eq. (5) to calculate the relative population of atoms in the  $^1P_1$  state,  $\rho_{^1P_1} \approx 0.027$ .

For the specific case of equal depths of all three blue detuned 1D lattices, and each of the depths equals to  $20 E^{\text{rec}}$  considered in the previous subsection, the intensity (averaged over time and space) of the 390 nm light experienced by the atoms passing the optical lattices periodic potentials, is  $\sim 2.1 \times 10^8 \text{ W/m}^2$ . The resulting loss coefficient (Eq. (4)) is equal to  $\gamma_P \approx 2.4 \times 10^5 \text{ s}^{-1}$ .

Assuming that blue MOT lifetime is limited by the collisions with the residual background gas molecules, the order of magnitude of the loss coefficient  $\gamma_{Sr}$  in rate Eqs. (1 - 3) in real experimental system can be approximated by the collisional loss rate due to the collisions with  $\text{H}_2$  reported in [54], resulting in  $\gamma_{Sr} \approx 0.4 \text{ s}^{-1}$  at the vacuum of  $10^{-9}$  mbar. The loss rate connected with atoms' decay to metastable  $^3P_2$  state in the case of operating blue MOT without repumpers is around  $35 \text{ s}^{-1}$ . Therefore, Eq. (3) shows that the blue MOT will be effectively depleted in the region where it overlaps with the 3D optical lattice trap made of three  $20 E^{\text{rec}}$  deep 1D optical lattices.

To overcome this loss of atoms, one can reduce the lattice intensity or even turn off the lattice beams during the blue MOT phase. Temporary switching off lattice light is technically feasible, e.g. with the power build-up cavity installed inside the vacuum setup on a low expansion glass spacer. The lattice laser can be safely switched back on and relocked during the red MOT phase, which lasts a few tens of ms. Another possibility is to store cold atoms during the blue MOT phase in the dark  $^3P_2$  state [55] or to use cold atomic beam loading directly the red MOT [56].

### Atoms trapped in the 3D optical lattice

After the interrogation of the clock transition, the populations of the ground and excited states are determined using the optical repumping through the  $^1P_1$  and  $^3S_1$  states, as discussed before. The effective intensity of the ionising light seen by an atom trapped in the motional ground state of the optical lattice is determined by the modulus of its wave function  $\psi$ , approximated in horizontal and vertical directions by Wannier and Wannier-Stark states, respectively. Due to the short lifetimes of the atoms in the  $^3S_1$  state, the spatial distribution of the atoms is determined by their preceding, metastable  $^3P_0$  state (the short lifetime prevents changing the shape of the distribution in the new potential corresponding to the  $^3S_1$  state polarisability before they decay to the lower states, which are not susceptible to photoionisation). The  $^{88}\text{Sr}$  atoms have the same polarisabilities in the  $^3P_0$  and  $^1S_0$  states at the optical trapping magic wavelength (at 389.889 nm these polarisabilities are equal to 459 a.u. as calculated using the data in Ref. [57]), therefore in our calculations, we have used numerically calculated Wannier and Wannier-Stark states for a given potential scaled in the units of  $E^{\text{rec}}$ .

The effective intensity from 1D lattice along  $\zeta$  axis is calculated by

$$I_{\text{eff},\zeta} = \int |\psi(\zeta)|^2 I(\zeta) d\zeta, \text{ with } \zeta = x, y, z, \quad (12)$$

where  $I(\zeta) = I_{0\zeta} \sin^2(k_\zeta \zeta)$  is the standing wave intensity distribution and  $I_{0\zeta}$  is the maximum intensity of each of 1D traps in  $\zeta$  direction. It should be pointed out that the effective intensity  $I_{\text{eff},\zeta}$  is calculated differently than the average intensity  $I_P$  from Eq. 7.  $I_P$  is the average intensity of light from a single non-reflected photoionization beam with Gaussian intensity distribution, whereas the  $I_{\text{eff},\zeta}$  is the effective intensity which induces photoionization of atoms in the ground Wannier or Wannier-Stark state of the blue-detuned optical lattice periodic potential.

Figure 8 depicts the dependence of the total effective intensity in 3D lattice  $I_{\text{eff}} = \sum_{\zeta} I_{\text{eff},\zeta}$  on the total amplitude of the potential  $3U_0$ . The blue crosses depict the values numerically calculated for Wannier-Stark (Wannier) states for the vertical (horizontal) directions in an optical lattice. In general, for deep enough optical lattice traps the calculations can be greatly simplified by approximating the system in Eq. (12) by a harmonic potential and its Gaussian ground states, which yields a square-root dependence of the effective intensity on the lattice potential (red crosses).

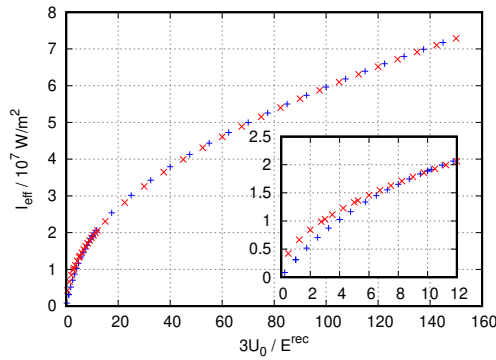


Fig. 8. The total effective intensity  $I_{\text{eff}}$  experienced by the atoms trapped in the motional ground state of a 3D blue-detuned magic wavelength optical lattice.  $I_{\text{eff}}$  values were calculated for Wannier-Stark (Wannier) states for the vertical (horizontal) directions in the optical lattice (blue crosses) and Gaussian states (red crosses) in a harmonic potential approximation.

In the considered lattice consisting of three independent 1D lattices, each  $20 E^{\text{rec}}$  deep, the  $I_{\text{eff}} \sim 4.6 \times 10^7 \text{ W/m}^2$ . To calculate the rate of losses for  $^3\text{S}_1$  state, we replace in Eq. 4 the average intensity  $I_P$  with the effective intensity  $I_{\text{eff}}$ . The resulting rate of losses of atoms in the  $^3\text{S}_1$  state due to photoionisation is  $1.26 \times 10^8 \text{ s}^{-1}$ , which is of the order of the  $^3\text{S}_1$  state decay rate due to the natural lifetime. Such a large loss rate significantly limits the applicability of the blue magic lattice with a  $^3\text{S}_1$ -based repumping scheme. A possible solution is to employ an alternative repumping scheme through the  $^3\text{D}_{1,2}$  states (see Fig. 1). As these  $^3\text{D}$  states lie below the photoionisation threshold for blue-detuned optical lattice, they are not affected by the photoionisation induced losses from 390 nm wavelength light. However, the high IR wavelengths of  $2.6 \mu\text{m}$  for the  $^3\text{P}_0$ - $^3\text{D}_1$  and  $3 \mu\text{m}$  for the  $^3\text{P}_2$ - $^3\text{D}_2$  transition make the use of these transitions experimentally challenging as the lasers at these wavelengths are often not readily available. Additionally, the longer lifetimes of  $\tau_{^3\text{D}_1} = 2.18(1) \mu\text{s}$  for  $^3\text{D}_1$  [1] and  $\tau_{^3\text{D}_2} = 12.7 \mu\text{s}$  for  $^3\text{D}_2$  state (the value deduced from the energy diagram in [51]) would require longer repumping times during the detection of the clock transition.

### 3.2.4. AC Stark shift from independent 1D lattices

To prevent interference between independent 1D lattices, small frequency detunings must exist between the light of each of the 1D lattices. While the detuning from the magic wavelength of the 1D lattice optical clock would add a considerable light shift to the clock frequency, in the 3D lattice the effective light shift can be still controlled at the required level. One can assume that the 1D optical lattice in the clock laser interrogation axis can be precisely tuned to the magic wavelength. With blue detuned optical lattice, all higher-order effects will be suppressed as atoms are trapped close to the intensity minimum. According to our calculations, a trapping depth of  $20 E^{\text{rec}}$  is enough for clock operations in the vertical direction. Tunnelling in horizontal directions do not have to be suppressed that well, and we assume individual trap depth to be  $20 E^{\text{rec}}$  as well. With the vertical lattice tuned to the magic wavelength, the required minimal detuning of two other individual lattice beams is determined by the atomic oscillation period and thus by the trap frequency. For a trapping depth of  $20 E^{\text{rec}}$ , the trap frequency is around 135 kHz. With detuning around a few times the trap frequency, we can assume that potential can trap atoms efficiently. Both horizontal lattice beams can be detuned to opposite sides of magic wavelength, which in case of identical intensity and almost perfectly linear light shift scaling around magic wavelength [19] should cancel out individual light shifts. If we assume detuning of plus and minus 500 kHz of each horizontal lattice beam and a relative intensity difference of 3%, the induced effective light shift from detuning from both horizontal lattice beams can be controlled to the level of around  $1 \times 10^{-19}$ . For both horizontal lattices detuned by 1 MHz and an intensity mismatch of 5%, the induced effective light shift is still around  $5 \times 10^{-19}$ . For this estimation, we use the dependence of the intensity seen by atoms calculated in subsection 3.2.3.

## 4. Conclusion

In conclusion, we have determined the values of the  $^{88}\text{Sr}$  photoionisation cross section at blue-detuned magic wavelength 389.889 nm to be  $2.20(50) \times 10^{-20} \text{ m}^2$  and  $1.38(66) \times 10^{-18} \text{ m}^2$ , for the excited states  $^1\text{P}_1$  and  $^3\text{S}_1$ , respectively. Additionally, we have measured the photoionisation cross section for the  $^1\text{P}_1$  state in a range from 378.4 nm to 407 nm and determined the position and the peak value of the autoionisation resonance ( $4d^2+5p^2$ )  $^1\text{D}_2$  to be 405.196(44) nm and  $5.20(94) \times 10^{-19} \text{ m}^2$ , respectively. These results are consistent with the results previously reported [35, 36], which, unlike ours, did not involve cold atomic systems.

To examine the potential feasibility of the blue-detuned magic wavelength strontium optical lattice trap, we have estimated photoionisation-induced atomic losses in a three-dimensional optical lattice trap operating at the minimal intensity required to fulfil the Lamb-Dicke regime [43, 44] for the clock transition. For a 3D lattice with lattice depths of  $20 E^{\text{rec}}$  we found the rate of

photoionization losses for  $^1P_1$  and  $^3S_1$  to be  $\gamma_P \approx 2.4 \times 10^5 \text{ s}^{-1}$  and  $1.26 \times 10^8 \text{ s}^{-1}$ , respectively, and we have compared these losses with other channels of atomic losses during the standard operation of an optical lattice strontium clock. We also make several suggestions on mitigating the photoionisation losses for  $^1P_1$  and  $^3S_1$  states, thus ensuring that neither of these loss channels is a critical defect for a blue-detuned lattice clock. In particular, the large photoionisation loss rate in the blue-detuned optical lattice makes the use of  $^3S_1$  state in the optical clock cycle unfeasible and would instead require the use of the less commonly  $^3D_1$  state which, while feasible, adds additional experimental difficulties due to the high IR wavelengths of the relevant  $^3P_0$ - $^3D_1$  and  $^3P_2$ - $^3D_2$  transitions.

Interestingly, the non-destructive measurements of the clock transition probability (e.g. [58,59]), assuming a different way of repumping, still seem compatible with the blue-detuned trap. The non-destructive measurements that utilise 461 nm light assume that the excited level is not populated thanks to detuning and low power of the local oscillator and probe beams (down to ~30 uW at the waist of ~75 um and detuning of ~2 GHz in the newest experiments, that corresponds to the relative population of atoms in the  $^1P_1$  state,  $\rho_{1P_1} \approx 0.00025$ ), because any atom in the excited  $^1P_1$  state in the optical lattice is lost from the relatively shallow optical trap.

Moreover, the schemes of a continuous superradiant optical active clocks that were proposed in [20] and related works that use a blue-detuned magic wavelength to realize the Lamb-Dicke regime are not using either the first-stage cooling or excitation readout in the presence of the blue-detuned optical lattice, therefore their feasibility is not affected by high photoionisation cross sections. The losses can, however, impact newer proposals, that would improve the proposed scheme by including repumping of superradiating atoms by external incoherent pumping [60,61].

## Funding

H2020 Future and Emerging Technologies (No 820404, iqClock project); The European Metrology Programme for Innovation and Research (EMPIR) Programme cofinanced by the Participating States and from the European Union's Horizon 2020 Research and Innovation Programme (EMPIR 17FUN03 USOQS); Fundacja na rzecz Nauki Polskiej (TEAM/2017-4/42); Narodowe Centrum Nauki (2017/25/B/ST2/00429, 2017/25/Z/ST2/03021).

## Acknowledgements

The measurements were performed at the National Laboratory FAMO (KL FAMO) in Toruń, Poland, and were supported by a subsidy from the Polish Ministry of Science and Higher Education.

## Disclosures

The authors declare no conflicts of interest.

## Data availability

Data underlying the results presented in this paper are available in the open data repository [62].

## References

1. T. Nicholson, S. Campbell, R. Hutson, G. Marti, B. Bloom, R. McNally, W. Zhang, M. Barrett, M. Safronova, G. Strouse, W. L. Tew, and J. Ye, "Systematic evaluation of an atomic clock at  $2 \times 10^{-18}$  total uncertainty," *Nat. Commun.* **6**, 6896 (2016).
2. M. Schioppa, R. C. Brown, W. F. McGrew, N. Hinkley, R. J. Fasano, K. Beloy, T. H. Yoon, G. Milani, D. Nicolodi, J. A. Sherman, N. B. Phillips, C. W. Oates, and A. D. Ludlow, "Ultrastable optical clock with two cold-atom ensembles," *Nat. Photonics* **11** (2016).
3. C. Lisdat, G. Grosche, N. Quintin, C. Shi, S. M. F. Raupach, C. Grebing, D. Nicolodi, F. Stefani, A. Al-Masoudi, S. Dörscher, S. Häfner, J.-L. Robyr, N. Chiodo, S. Bilicki, E. Bookjans, A. Koczwara, S. Koke, A. Kuhl, F. Wiotte, F.

- Meynadier, E. Camisard, M. Abgrall, M. Lours, T. Legero, H. Schnatz, U. Sterr, H. Denker, C. Chardonnet, Y. Le Coq, G. Santarelli, A. Amy-Klein, R. Le Targat, J. Lodewyck, O. Lopez, P.-E. Pottie, "A clock network for geodesy and fundamental science," *Nat. Commun.* **7**, 12443 (2016).
4. J. Grotti, S. Koller, S. Vogt, S. Häfner, U. Sterr, C. Lisdat, H. Denker, C. Voigt, L. Timmen, A. Rolland, F. N. Baynes, H. S. Margolis, M. Zampaolo, P. Thoumany, M. Pizzocaro, B. Rauf, F. Bregolin, A. Tampellini, P. Barbieri, M. Zucco, G. A. Costanzo, C. Clivati, F. Levi, and D. Calonico, "Geodesy and metrology with a transportable optical clock," *Nat. Phys.* **14** (2018).
  5. M. Takamoto, I. Ushijima, N. Ohmae, T. Yahagi, K. Kokado, H. Shinkai, and H. Katori, "Test of general relativity by a pair of transportable optical lattice clocks," *Nat. Photonics* (2020).
  6. P. Delva, J. Lodewyck, S. Bilicki, E. Bookjans, G. Vallet, R. Le Targat, P.-E. Pottie, C. Guerlin, F. Meynadier, C. Le Poncin-Lafitte, O. Lopez, A. Amy-Klein, W.-K. Lee, N. Quintin, C. Lisdat, A. Al-Masoudi, S. Dörscher, C. Grebing, G. Grosche, A. Kuhl, S. Raupach, U. Sterr, I. R. Hill, R. Hobson, W. Bowden, J. Kronjäger, G. Marra, A. Rolland, F. N. Baynes, H. S. Margolis, and P. Gill, "Test of Special Relativity Using a Fiber Network of Optical Clocks," *Phys. Rev. Lett.* **118**, 221102 (2017).
  7. P. Wcisło, P. Morzyński, M. Bober, A. Cygan, D. Lisak, R. Ciuryło, and M. Zawada, "Experimental constraint on dark matter detection with optical atomic clocks," *Nat. Astron.* **1**, 0009 (2016).
  8. P. Wcisło, P. Ablewski, K. Beloy, S. Bilicki, M. Bober, R. Brown, R. Fasano, R. Ciuryło, H. Hachisu, T. Ido, J. Lodewyck, A. Ludlow, W. McGrew, P. Morzyński, D. Nicolodi, M. Schioppo, M. Sekido, R. Le Targat, P. Wolf, X. Zhang, B. Zjawin, and M. Zawada, "New bounds on dark matter coupling from a global network of optical atomic clocks," *Sci. Adv.* **4** (2018).
  9. B. M. Roberts, P. Delva, A. Al-Masoudi, A. Amy-Klein, C. Bærentsen, C. F. A. Baynham, E. Benkler, S. Bilicki, S. Bize, W. Bowden, J. Calvert, V. Cambier, E. Cantin, E. A. Curtis, S. Dörscher, M. Favier, F. Frank, P. Gill, R. M. Godun, G. Grosche, C. Guo, A. Hees, I. R. Hill, R. Hobson, N. Huntemann, J. Kronjäger, S. Koke, A. Kuhl, R. Lange, T. Legero, B. Lipphardt, C. Lisdat, J. Lodewyck, O. Lopez, H. S. Margolis, H. Álvarez-Martínez, F. Meynadier, F. Ozimek, E. Peik, P.-E. Pottie, N. Quintin, C. Sanner, L. D. Sarlo, M. Schioppo, R. Schwarz, A. Silva, U. Sterr, C. Tamm, R. L. Targat, P. Tuckey, G. Vallet, T. Waterholter, D. Xu, and P. Wolf, "Search for transient variations of the fine structure constant and dark matter using fiber-linked optical atomic clocks," *New J. Phys.* **22**, 093010 (2020).
  10. C. J. Kennedy, E. Oelker, J. M. Robinson, T. Bothwell, D. Kedar, W. R. Milner, G. E. Marti, A. Derevianko, and J. Ye, "Precision metrology meets cosmology: Improved constraints on ultralight dark matter from atom-cavity frequency comparisons," *Phys. Rev. Lett.* **125**, 201302 (2020).
  11. C. Shi, J.-L. Robyr, U. Eismann, M. Zawada, L. Lorini, R. Le Targat, and J. Lodewyck, "Polarizabilities of the  $^{87}\text{Sr}$  clock transition," *Phys. Rev. A* **92**, 012516 (2015).
  12. T. Middelmann, S. Falke, C. Lisdat, and U. Sterr, "High Accuracy Correction of Blackbody Radiation Shift in an Optical Lattice Clock," *Phys. Rev. Lett.* **109**, 263004 (2012).
  13. K. Gibble, "Scattering of Cold-Atom Coherences by Hot Atoms: Frequency Shifts from Background-Gas Collisions," *Phys. Rev. Lett.* **110**, 180802 (2013).
  14. K. Gibble and B. J. Verhaar, "Eliminating cold-collision frequency shifts," *Phys. Rev. A* **52**, 3370–3373 (1995).
  15. S. Gupta, Z. Hadzibabic, M. W. Zwierlein, C. A. Stan, K. Dieckmann, C. H. Schunck, E. G. M. van Kempen, B. J. Verhaar, and W. Ketterle, "Radio-Frequency Spectroscopy of Ultracold Fermions," *Science* **300**, 1723–1726 (2003).
  16. I. Ushijima, M. Takamoto, M. Das, T. Ohkubo, and H. Katori, "Cryogenic optical lattice clocks," *Nat. Photonics* **9**, 185–189 (2015).
  17. H. Katori, M. Takamoto, V. G. Pal'chikov, and V. D. Ovsiannikov, "Ultrastable Optical Clock with Neutral Atoms in an Engineered Light Shift Trap," *Phys. Rev. Lett.* **91**, 173005 (2003).
  18. I. Ushijima, M. Takamoto, and H. Katori, "Operational Magic Intensity for Sr Optical Lattice Clocks," *Phys. Rev. Lett.* **121**, 263202 (2018).
  19. M. Takamoto, H. Katori, S. I. Marmo, V. D. Ovsiannikov, and V. G. Pal'chikov, "Prospects for Optical Clocks with a Blue-Detuned Lattice," *Phys. Rev. Lett.* **102**, 063002 (2009).
  20. G. A. Kazakov and T. Schumm, "Active optical frequency standard using sequential coupling of atomic ensembles," *Phys. Rev. A* **87**, 013821 (2013).
  21. A. D. Ludlow, M. M. Boyd, J. Ye, E. Peik, and P. O. Schmidt, "Optical atomic clocks," *Rev. Mod. Phys.* **87**, 637–701 (2015).
  22. M. Takamoto, F.-L. Hong, R. Higashi, and H. Katori, "An optical lattice clock," *Nature* **435**, 321–324 (2005).
  23. A. D. Ludlow, M. M. Boyd, T. Zelevinsky, S. M. Foreman, S. Blatt, M. Notcutt, T. Ido, and J. Ye, "Systematic study of the  $^{87}\text{Sr}$  clock transition in an optical lattice," *Phys. Rev. Lett.* **96**, 033003 (2006).
  24. T. Takano, R. Mizushima, and H. Katori, "Precise determination of the isotope shift of  $^{88}\text{Sr}$ - $^{87}\text{Sr}$  optical lattice clock by sharing perturbations," *Appl. Phys. Express* **10**, 072801 (2017).
  25. M. Bober, P. Morzyński, A. Cygan, D. Lisak, P. Masłowski, M. Prymaczek, P. Wcisło, P. Ablewski, M. Piwiński, S. Wójtewicz, K. Bielska, D. Bartoszek-Bober, R. S. Trawiński, M. Zawada, R. Ciuryło, J. Zachorowski, M. Piotrowski, W. Gawlik, F. Ozimek, and C. Radzewicz, "Strontium optical lattice clocks for practical realization of the metre and secondary representation of the second," *Meas. Sci. Technol.* **26**, 075201 (2015).
  26. H. G. Dehmelt, "Monoion oscillator as potential ultimate laser frequency standard," *IEEE Transactions on Instrumentation Meas.* **IM-31**, 83–87 (1982).
  27. T. P. Dinneen, C. D. Wallace, K.-Y. N. Tan, and P. L. Gould, "Use of trapped atoms to measure absolute photoionization

- cross sections,” *Opt. Lett.* **17**, 1706–1708 (1992).
28. M. Witkowski, R. Munoz-Rodriguez, A. Raczynski, J. Zaremba, B. Nagórny, P. S. Żuchowski, R. Ciuryło, and M. Zawada, “Photoionization cross sections of the  $5S_{1/2}$  and  $5P_{3/2}$  states of Rb in simultaneous magneto-optical trapping of Rb and Hg,” *Phys. Rev. A* **98**, 053444 (2018).
  29. C. Gabbanini, S. Gozzini, and A. Lucchesini, “Photoionization cross section measurement in a Rb vapor cell trap,” *Opt. Commun.* **141**, 25 – 28 (1997).
  30. G. Ferrari, R. E. Drullinger, N. Poli, F. Sorrentino, and G. M. Tino, “Cooling of Sr to high phase-space density by laser and sympathetic cooling in isotopic mixtures,” *Phys. Rev. A* **73**, 023408 (2006).
  31. M. H. Shah, H. A. Camp, M. L. Trachy, G. Veshapidze, M. A. Gearba, and B. D. DePaola, “Model-independent measurement of the excited fraction in a magneto-optical trap,” *Phys. Rev. A* **75**, 053418 (2007).
  32. P. Ewart and A. F. Purdie, “Laser ionization spectroscopy of Rydberg and autoionization levels in Sr I,” *J. Phys. B* **9**, 437–441 (1976).
  33. P. Esherick, “Bound, even-parity  $J = 0$  and  $J = 2$  spectra of Sr,” *Phys. Rev. A* **15**, 1920–1936 (1977).
  34. M. Baig, M. Yaseen, R. Ali, A. Nadeem, and S. Bhatti, “Near-threshold photoionization spectra of strontium,” *Chem. Phys. Lett.* **296**, 403 – 407 (1998).
  35. W. Mende, K. Bartschat and M. Kock, “Near-threshold photoionization from the Sr I ( $5s5p$ ) $^1P_1^o$  state,” *J. Phys. B: At. Mol. Opt. Phys.* **28**, 2385–2393 (1995).
  36. S. ul Haq, S. Mahmood, N. Amin, Y. Jamil, R. Ali, and M. A. Baig, “Measurements of photoionization cross sections from the  $5s5p$   $^1P_1$  and  $5s6s$   $^1S_0$  excited states of strontium,” *J. Phys. B: At. Mol. Opt. Phys.* **39**, 1587–1596 (2006).
  37. U. Fano, “Effects of Configuration Interaction on Intensities and Phase Shifts,” *Phys. Rev.* **124**, 1866–1878 (1961).
  38. G. García and J. Campos, “Transition probabilities for triplet levels of Sr(I),” *J. Quant. Spectrosc. Radiat. Transf.* **39**, 477–483 (1988).
  39. G. Jönsson, C. Levinson, A. Persson, and C. G. Wahlström, “Natural radiative lifetimes in the  $^1P_1$  and  $^1F_3$  sequences of Sr I,” *Z. Rev. A* **316**, 255–258 (1984).
  40. S. G. Porsev, A. D. Ludlow, M. M. Boyd, and J. Ye, “Determination of Sr properties for a high-accuracy optical clock,” *Phys. Rev. A* **78**, 032508 (2008).
  41. S. Will, *From atom optics to quantum simulation. Interacting bosons and fermions in three-dimensional optical lattice potentials* (Springer-Verlag Berlin Heidelberg, 2013).
  42. S. L. Campbell, R. B. Hutson, G. E. Marti, A. Goban, N. Darkwah Oppong, R. L. McNally, L. Sonderhouse, J. M. Robinson, W. Zhang, B. J. Bloom, and J. Ye, “A fermi-degenerate three-dimensional optical lattice clock,” *Science* **358**, 90–94 (2017).
  43. R. H. Dicke, “The effect of collisions upon the doppler width of spectral lines,” *Phys. Rev.* **89**, 472–473 (1953).
  44. D. J. Wineland and W. M. Itano, “Laser cooling of atoms,” *Phys. Rev. A* **20**, 1521–1540 (1979).
  45. P. Lemonde and P. Wolf, “Optical lattice clock with atoms confined in a shallow trap,” *Phys. Rev. A* **72**, 033409 (2005).
  46. G. H. Wannier, “Wave functions and effective hamiltonian for bloch electrons in an electric field,” *Phys. Rev.* **117**, 432–439 (1960).
  47. M. Glück, A. R. Kolovsky, and H. J. Korsch, “Wannier–Stark resonances in optical and semiconductor superlattices,” *Phys. Reports* **366**, 103 – 182 (2002).
  48. G. Tackmann, B. Pelle, A. Hilico, Q. Beaufils, and F. Pereira dos Santos, “Raman-laser spectroscopy of wannier-stark states,” *Phys. Rev. A* **84**, 063422 (2011).
  49. T. Bothwell, C. Kennedy, A. Aeppli, D. Kedar, J. Robinson, E. Oelker, A. Staron, and J. Ye, “Resolving the gravitational redshift across a millimetre-scale atomic sample,” *Nature* **602**, 420–424 (2022).
  50. Courtillot, I., Quessada-Vial, A., Bruschi, A., Kolker, D., Rovera, G. D., and Lemonde, P., “Accurate spectroscopy of Sr atoms,” *Eur. Phys. J. D* **33**, 161–171 (2005).
  51. P. G. Mickelson, Y. N. M. de Escobar, P. Anzel, B. J. DeSalvo, S. B. Nagel, A. J. Traverso, M. Yan, and T. C. Killian, “Repumping and spectroscopy of laser-cooled Sr atoms using the  $(5s5p)3P_2$ – $(5s4d)3D_2$  transition,” *J. Phys. B: At. Mol. Opt. Phys.* **42**, 235001 (2009).
  52. S. Zhang, P. Ramchurn, M. Menchetti, Q. Ubaid, J. Jones, K. Bongs, and Y. Singh, “Novel repumping on  $3P_0 \rightarrow 3D_1$  for Sr magneto-optical trap and Landé g factor measurement of  $3D_1$ ,” *J. Phys. B: At. Mol. Opt. Phys.* **53**, 235301 (2020).
  53. X. Baillard, M. Fouché, R. L. Targat, P. G. Westergaard, A. Lecallier, Y. L. Coq, G. D. Rovera, S. Bize, and P. Lemonde, “Accuracy evaluation of an optical lattice clock with bosonic atoms,” *Opt. Lett.* **32**, 1812–1814 (2007).
  54. M. Abdel-Hafiz, P. Ablewski, A. Al-Masoudi, H. Álvarez Martínez, P. Balling, G. Barwood, E. Benkler, M. Bober, M. Borkowski, W. Bowden, R. Ciuryło, H. Cybulski, A. Didier, M. Doležal, S. Dörscher, S. Falke, R. M. Godun, R. Hamid, I. R. Hill, R. Hobson, N. Huntemann, Y. Le Coq, R. Le Targat, T. Legero, T. Lindvall, C. Lisdat, J. Lodewyck, H. S. Margolis, T. E. Mehlstäubler, E. Peik, L. Pelzer, M. Pizzocaro, B. Rauf, A. Rolland, N. Scharnhorst, M. Schioppa, P. O. Schmidt, R. Schwarz, Ç. Şenel, N. Spethmann, U. Sterr, C. Tamm, J. W. Thomsen, A. Vianello, and M. Zawada, “Guidelines for developing optical clocks with  $10^{-18}$  fractional frequency uncertainty,” arXiv e-prints arXiv:1906.11495 (2019).
  55. S. Stellmer, M. K. Tey, B. Huang, R. Grimm, and F. Schreck, “Bose-Einstein Condensation of Strontium,” *Phys. Rev. Lett.* **103**, 200401 (2009).
  56. C.-C. Chen, S. Bennetts, R. G. Escudero, B. Pasquiou, and F. Schreck, “Continuous Guided Strontium Beam with

- High Phase-Space Density,” *Phys. Rev. Appl.* **12**, 044014 (2019).
57. X. Zhou, X. Xu, X. Chen, and J. Chen, “Magic wavelengths for terahertz clock transitions,” *Phys. Rev. A* **81**, 012115 (2010).
  58. G. Vallet, E. Bookjans, U. Eismann, S. Bilicki, R. L. Targat, and J. Lodewyck, “A noise-immune cavity-assisted non-destructive detection for an optical lattice clock in the quantum regime,” *New J. Phys.* **19**, 083002 (2017).
  59. R. Hobson, W. Bowden, A. Vianello, I. R. Hill, and P. Gill, “Cavity-enhanced non-destructive detection of atoms for an optical lattice clock,” *Opt. Express* **27**, 37099–37110 (2019).
  60. C. Hotter, D. Plankensteiner, L. Ostermann, and H. Ritsch, “Superradiant cooling, trapping, and lasing of dipole-interacting clock atoms,” *Opt. Express* **27**, 31193–31206 (2019).
  61. A. Bychek, C. Hotter, D. Plankensteiner, and H. Ritsch, “Superradiant lasing in inhomogeneously broadened ensembles with spatially varying coupling [version 2; peer review: 2 approved],” *Open Res. Eur.* **1** (2021).
  62. W. Marcin, B. Sławomir, M. Bober, D. Kovačić, V. Singh, A. Tonoyan, and M. Zawada, “Photoionisation losses in a strontium optical lattice clock operating at blue-detuned magic wavelength light,” (2022). RepOD <https://doi.org/10.18150/LQ6WUK>.